The Cryosphere Discuss., 6, 4417–4446, 2012
www.the-cryosphere-discuss.net/6/4417/2012/
doi:10.5194/tcd-6-4417-2012

The Cryosphere Discussions

Multi decadal glacier area fluctuations in Pan-Arctic

S. H. Mernild[1] and J. K. Malmros[2]

[1]Climate, Ocean, and Sea Ice Modeling Group, Los Alamos National Laboratory, New Mexico, USA
[2]Centro de Estudios Científicos (CECs), Valdivia, Chile

Received: 30 August 2012 – Accepted: 9 October 2012 – Published: 16 October 2012

Correspondence to: S. H. Mernild (mernild@lanl.gov)

Published by Copernicus Publications on behalf of the European Geosciences Union.

Abstract

The shrinking of land-terminating glaciers and ice caps (GIC) has been documented in high-latitude regions, even though repeat observations upon which to base such studies have been limited in space. Here, we present a new record of satellite-derived area changes for 321 land-terminating GIC throughout Pan-Arctic and for the W. Canada and W. US, with focus on the period from mid-1980s to late-2000s/2011 (the last ca. 25 yr). The mean shrinking rate was $-0.06 \pm 0.01\,\mathrm{km^2\,yr^{-1}}$ during a period with climate warming. Most of the observed GIC shrank in area, more so than previously believed: while only 8 % advanced. The analysis indicates that the observed GIC have lost an arithmetic average of one-fifth of their area since the mid-1980s (equal to a shrinking rate of ca. $-1\,\%\,\mathrm{yr^{-1}}$), with the highest rate of loss of $-40 \pm 4\,\%$ ($-1.7\,\%\,\mathrm{yr^{-1}}$) in Alaska, and the lowest rate of loss of $-12 \pm 3\,\%$ ($-0.5\,\%\,\mathrm{yr^{-1}}$) in Arctic Russia.

1 Introduction

Land-terminating glaciers and ice caps (henceforth GIC) excluding the Greenland Ice Sheet (GrIS) and the Antarctic Ice Sheet (AIS) are tracers of climate warming, as air temperature and precipitation changes control the surface mass balance, and subsequently the volume and area exposure (Kaser et al., 2006; Bloch et al., 2010; Bjork et al., 2012; Cogley, 2012; Mernild et al., 2012a). The average rise in air temperature of recent decades has been more pronounced at high latitudes than globally (Hansen et al., 2010), resulting in thinning and shrinking of GIC (Meier et al., 2007; Bahr et al., 2009; Dyurgerov, 2010; WGMS, 2011). Even without additional warming, land-terminating GIC will lose an estimated $30 \pm 5\,\%$ of their area to reach equilibrium with the climate of the past decade, due to the delayed response of GIC to climate warming (Mernild et al., 2012a).

Around half of the estimated GIC surface area and two-third of its volume are found in the Pan-Arctic region (Radić and Hock, 2010), highlighting a need to observe and

TCD
6, 4417–4446, 2012

map the relation between GIC changes and on-going climate warming, following the warmest decade (2001–2010) on record (Hansen et al., 2010). Currently, GIC retreat and mass loss are raising the eustatic global sea-level by approximately 1 mm yr^{-1}, in the same range as the combined GrIS and AIS sea-level contribution (Meier et al., 2007; Radić and Hock, 2011).

Time series of frontal position and area of GIC have become far more extensive in the satellite era (Yde and Knudsen, 2007; Bjork et al., 2012; Bloch et al., 2012; Cogley, 2012; Mernild et al., 2012b). Only a small fraction of the Pan-Arctic's GIC has been directly observed in-situ, even though thousands of individual GIC are located in the Arctic (Weidick et al., 1992). There is a need for information about contemporary GIC area fluctuations and their correspondence with climate. Recent analyses (Yde and Knudsen, 2007; Kaser et al., 2006; Bloch et al., 2010; Bjork et al., 2012; Cogley 2012; Kargel et al., 2012; Mernild et al., 2012b) of GIC fluctuations and area exposures in Pan-Arctic, e.g., in W. and SE. Greenland and W. Canada and W. US, based on historical accounts and aerial and satellite images of the late twentieth century and to present, have suggested that the GIC area shrinking rate on average is −0.04 km^2 yr^{-1}, or −0.1 to −0.5 % yr^{-1} and up to −1 % yr^{-1} comparable to rates reported for high-latitude mountain ranges (Bloch et al., 2010).

Here, for the period mid-1980s to late-2000s/2011 we examine net area fluctuations and shrinking rates using multispectral Landsat satellite data for 321 land-terminating GIC, divided into seven (first-order) glaciated regions: Alaska, W. Canada and W. US, Arctic Canada, Greenland, Scandinavia, Arctic Russia, and N. and E. Asia, and further divided into 12 sub-regions. Area changes were considered in the context of observed air temperature time series. Finally, we investigate differences in GIC initial area versus GIC area change, and we calculate the percentage of area advancing GIC.

TCD
6, 4417–4446, 2012

2 Methods and data set

2.1 The satellite method

The satellite-derived GIC planimetric area data set was obtained from high spatial resolution Landsat-5 TM (Thematic Mapper) and Landsat-7 ETM+ (Enhanced Thematic Mapper Plus) imagery from 28 scenes, having a ground resolution of 30 m (Table 1). The satellite data set was: (1) obtained from a pair of Landsat scenes covering the same region, recorded at least ten years apart and with end scenes obtained no earlier than 2003 (within the last decade); (2) acquired during the end-of the ablation season, typically from end-of July through end-of September, to minimize snow-cover interference (only GIC larger than 0.028 km^2 were mapped to avoid snow patches to be included in the data set); (3) obtained from cloud-free areas, on scenes with less than 50 % cloud-cover; (4) visually inspected before use in the supervised classification process to avoid misclassification caused by heavy snow covered scenes; (5) when using Landsat-7 ETM+ (2003 to present) subject to the Scan Line Instrument (SLI) malfunction, two (approximate same date) scenes were combined to replace gaps; and (6) obtained where the SLI failure would not influence the GIC area estimation.

Data from twelve Pan-Arctic sub-regions were acquired (Fig. 1): however, not from Svalbard and Iceland due to the lack of scenes meeting the selection criteria. All the Landsat scenes were projected in World Geodetic System 1984 (WGS84), atmospherically and radiometrically calibrated using the Landsat calibration tool in ENVI™ software package (http://www.ittvis.com/ProductServices/ENVI.aspx), converting the band values to "At Surface Reflectance". The individual bands (TM and ETM+ bands 1–5, and (7) were standardized using the ENVI™ Dark Subtract (DS) tool before ratios and indices were calculated.

The supervised classification process used for the scenes was based on a multi-criteria analysis involving the calculation of a set of indices (Fig. 2) (Mernild et al., 2012b) (the indices and calculations were carried out using the "Bandmath" tool in

TCD
6, 4417–4446, 2012

ENVI™ software package): normalized difference snow index (NDSI) (Hall et al., 1995); normalized difference water index (NDWI) (Gao, 1996); normalized difference vegetation index (NDVI) (Rouse et al., 1973); and Ratio TM/ETM + bands (3/5) (Visible light/Short Wave Infrared). The ratio introduced by Crane and Anderson (1984), and Dozier and Marks (1987). The ratio between bands 3 and 5 was found to produce better contrast across the mountainous regions than the often applied TM/ETM + bands (2/5) ratio. The Ratio was used in reference due to better performance than the NDSI index in mountainous areas capturing ice and snow covered areas influenced by shadows and debris (Paul, 2004).

The NDVI was used to filter out vegetation and the NDWI to identify and filter out lakes in the margin area of the GIC. The resulting classifications were converted to polygon files representing the GIC area, and where needed the extent were manually edited in ESRI™ ArcMap. For each GIC, the GIC margin positions were digitized for both the beginning and end of the observation period and the area shrinkage/advance rates were calculated. An example of GIC area estimations is illustrated in Fig. 3, where the margin positions were digitized for a specific glacier for both 1986 and 2011 (ID # L29, SE. Greenland; the location of L29 can be seen in Mernild et al. (2012b; Fig. 1), and the shrinking rate calculated.

The indices threshold input values used in the individual classification scenes varied across the regions and years, as a result of the inherent reflective properties due to changes in the surfaces structure over time. The individual threshold values were selected based on the best performance in identifying elements like snow/ice, vegetation, and water (NDSI: 0.4–0.5, NDVI: 0.25–0.35, NDWI: 0.2–0.5). As an example, changes in vegetation were due to both changes in seasonal and in regional variability, and for snow cover due to compaction and wetness (Brest, 1987; Hall et al., 2001), making it difficult to apply an all-round calcification algorithm that works everywhere at any time.

For specific sub-regions the following deviations occurred due to the classification process:

TCD
6, 4417–4446, 2012

– For W. Canada and W. US, only GIC not interrupted by the gaps in the Landsat-7 scene was included.

– For Bolshevik Island, GIC influenced by the Landsat-7 gaps were carefully digitized, and finalized using visual interpretation based on the 1985 Landsat-5 scene. GIC ID # 1 was divided, due to extensive cloud cover, at the same location in both scenes, therefore only representing the majority of the glacier.

– For Novaya Zemlya the Landsat-5 scene was warped in ArcMap to fit the Landsat-7 scene due to gaps in the classification (SLI failure) (of 1.2 m due to the root mean square (RMS), based on 26 ground control points (GCP)). The 1987 classification had the Landsat-7 gap area removed, so the GIC areas could be compared with the 2011 classification.

– For NW. Greenland GIC ID # 23 was divided, due to the scene coverage, at the same location in both scenes (for 1987 and 2006), and therefore only representing most of the GIC within the scene.

2.2 Satellite uncertainties

The overall raw classification errors (misclassifications) for each year were found by comparison with the cleaned up classification and estimated to be 4.9 % (overestimate by 3.0 % due to snow patches and underestimate by 1.9 % due to heavily debris covered terrain and shadow regions) (Table 2). The highest error values were found in Alaska and W. Canada and W. US caused by shadow effects due to terrain elevations, where the errors were underestimated by 3.1 % and 3.2 %, respectively. For both S. Scandinavia and Kamchatka it was due to snow patches, where the errors were overestimated by 3.7 % and 3.9 %, respectively. Overall for troublesome regions Alaska, W. Canada and W. US, S. Scandinavia, and Kamchatka the classification error were 6.2, 6.0, 5.3, and 6.0 %, respectively. In Table 2 error values are listed for the individual sub-regions.

TCD
6, 4417–4446, 2012

Standard pixel errors associated with the different scenes and sensors in relation to the classification process was expected to be half the pixel size: ±15 m for both TM and ETM+ (Table 1) (Hall et al., 2003; Mernild et al., 2012b). As a test e.g., the Landsat-derived Mittivakkat Gletscher margin, SE. Greenland, was validated against direct GPS margin observations from 2011, indicating an overall root mean square (RMS) difference of 22 m between Landsat-7 satellite-derived and GPS margin observations (Mernild et al., 2012b).

2.3 The data set

We have compiled a data set of Landsat satellite-derived planimetric area change for 321 land-terminating GIC in Pan-Arctic and for the W. Canada and W. US (henceforth Pan-Arctic), between 52.4° N and 89.3° N latitude, from mid-1980s to late-2000s/2011: the compiled GIC area corresponds to 1 % of the estimated Pan-Arctic GIC area (Radić and Hock, 2010). The 321 GIC from the compiled data set were chosen to follow (significantly; herein the term "significantly" is only used for which the relationship is statistically significant at the 10 % level or better, based on a linear regression t-test) the area GIC distribution found in the Randolph Glacier Inventory (RGI) v. 2.0 data set (between 52.4° N and 89.3° N latitude, and GIC larger than 0.028 km^2) (Arendt et al., 2012) (see histogram in Fig. 4). Even though the compiled data set have a few percentage less small glaciers (< 5 km^2) and more large glaciers (> 5 km^2) compared to RGI, the compiled data set appears, due to the size distribution, to be representative for Pan-Arctic GIC, where the smallest bins (below 5 km^2) contain a non-trivial amount of the total GIC mass (Bahr and Radić, 2012).

The GIC were compiled from seven first-order regions for the period mid-1980s to late-2000s/2011: Alaska (GIC, $n = 26$), W. Canada and W. US (31), Arctic Canada (32), Greenland (104), Scandinavia (60), Arctic Russia (47), and N. and E. Asia (21) (for N. and E. Asia the observation period covered the period 1999 to 2011) (Table 3), where Greenland was divided into four sub-regions (NE. (29), SE. (35), SW. (17), and NW. (23)), and both Scandinavia (N. (29) and S. (31)) and Arctic Russia into two sub-regions

TCD
6, 4417–4446, 2012

(Novaya Zemlya (21) and Bolshevik Island (26)), ending up in total with twelve Pan-Arctic sub-regions (the sub-regions are shown on Fig. 1 and Table 4). The exact observation periods are illustrated on the first-order regional scale in Table 3. In Table 4 values are illustrated on sub-regional scale.

3 Results and discussion

3.1 GIC initial area versus GIC area change

The compiled data set illustrates a significant trend (Fig. 4), where it can be concluded for both advancing ($r^2 = 0.56$) and shrinking GIC ($r^2 = 0.75$), that the largest observed GIC (km^2) are the ones having the greatest absolute advancing or shrinking area rates per year ($km^2\,yr^{-1}$): For the minor GIC this absolute trend is vice versa. The change in area is influenced by the initial GIC size, where large GIC lost the highest absolute values (Fig. 4) and small GIC lost the highest relative values (Fig. 5). Small GIC between 0.1 to 5.0 km^2 lost in average between −21 to −27 % of the area, and for advancing GIC, the small GIC between 0.1 and 1.0 km^2 were the ones having the greatest average percentage of area increase of 13 to 17 % (Fig. 5). Different theories have been mentioned in Liston (1999), Granshaw et al. (2006), Demuth et al. (2008), Tennant et al. (2012), analyzing why the small GIC lost the greatest percentage of their area. This trend is probably because: (1) large GIC are usually characterized by huge variability in thickness, while small GIC are typically thinner and the thicknesses more uniform. As a consequence, the fractional area loss rates for the large GIC is relatively slow, while the fractional area loss rates for small GIC is relatively fast; (2) a high area-to-volume ratio, indicating that for the same ablation rate small GIC should shrink faster; and/or (3) a possible higher perimeter-to-area ratio which makes the small GIC more affected to reflection radiation and convection of heat from the surrounding areas. GIC smaller the 0.1 km^2 faced less percentage of area loss than GIC between 0.1 to 5.0 km^2 (Fig. 5), probably because the smallest GIC tended to be located in more sheltered

TCD
6, 4417–4446, 2012

locations with the possibility for reduced insolation (DeBeer and Sharp, 2007; Demuth et al., 2008). However, the understanding of the link between initial area (km^2) and area changes ($km^2\ yr^{-1}$), and why the shrinking rates depend on the initial area is still one of the gaps in our understanding of GIC behavior (Cogley, 2012).

3.2 Area change – retreat and advance

Throughout the ca. 25 yr of satellite coverage, the Pan-Arctic GIC have faced widespread non-uniform shrinkage, where 8 %, 26 out of the 321 observed GIC advanced in area (Figs. 1, 6, and 7). As an example, these non-uniform GIC area changes are illustrated for twelve individual GIC (for both minor and major GIC) (Fig. 8), where ten out of twelve GIC showed retreat. On sub-regional scale, half of the twelve regions showed GIC retreated for all observed GIC, whereas 5 % of the GIC advanced in Novaya Zemlya, 9 % SE. Greenland (Mernild et al., 2012b), 10 % Kamchatka, 13 % W. Canada and W. US, 37 % SW. Greenland, and 42 % Bolshevik Island (Table 4). The GIC area changes in Bolshevik Island are not detailed described in general in the literature, therefore it is difficult to conclude whether the GIC advancement are due to a response from a positive net mass balance (climatic response), or due to surging activities (climate-dynamic GIC response), however all the GIC in Bolshevik Island are facing north. Advancing GIC have also been recognized in other regions, however they are located apart from surge clusters, e.g., for W. Canada and W. US (Post, 1969), SW. Greenland (Yde and Knudsen, 2007), and SE. Greenland (Jiskoot et al., 2003), indicating that the GIC likely are influenced by climate impacts. Common for the advancing GIC are, for all sub-regions, that they predominantly are facing north (85 %), and that they were influenced by dynamic response to changes in positive mass balance and climate, except for GIC located in Arctic Russia or Kamchatka, where surging activities are present (Grant et al., 2009). For example, for Novaya Zemlya 5 % of the observed GIC advanced (Table 4), identical with the percentage of surging GIC stated by Grant et al. (2009), where 32 potential surge-types of GIC were identified out of 692 GIC on the Novaya Zemlya archipelago.

TCD
6, 4417–4446, 2012

For the compiled data set the highest frequency (number of observations) of GIC area change occurred within the interval from −5 to −20 % (see histogram in Fig. 7), overall spanning from a shrinkage of −99 % to an advance of 37 %, with an arithmetic mean relative GIC area change of −21 ± 1 % (here and below, the error term is stated as plus or minus one standard error) (Fig. 7). Without including area losses for the very largest GIC (GIC > 340 km^2; Fig. 5), we are likely to overestimate the overall relatively rate of area loss, however insignificantly. On the regional scale Alaska faced an average GIC shrinkage of −40 ± 4 % (−1.7 % yr^{-1}), Arctic Canada −35 ± 4 % (−1.7 % yr^{-1}), N. and E. Asia −23 ± 3 % (−1.9 % yr^{-1}), Scandinavia −21 ± 2 % (−0.9 % yr^{-1}), Greenland −20 ± 2 % (−0.8 % yr^{-1}), W. Canada and W. US −12 ± 3 % (−0.5 % yr^{-1}), and Arctic Russia −12 ± 2 % (−0.5 % yr^{-1}) (Fig. 9 and Table 3). For W. Canada and W. US, more specifically for the Canadian Rocky Mountains, an area shrinkage of −15 to −25 % (ca. 1950–2000) was computed (Luckman and Kavavagh, 2000, DeBeer and Sharp, 2007), but a direct comparison to previous studies can not be done, due to the uneven observation periods.

The arithmetic mean area shrinkage for the compiled data set corresponds to ca. one-fifth of the mid-1980s GIC area, equal to a mean GIC area shrinking rate of −0.06 ± 0.01 $km^2\,yr^{-1}$ (Tables 3 and 4): a higher rate than illustrated in earlier studies (Mernild et al., 2012b). On a sub-regional scale the absolute arithmetic mean shrinking rate was highest for NW. Greenland −0.18 $km^2\,yr^{-1}$, Novaya Zemlya −0.16 $km^2\,yr^{-1}$, and Ellesmere Island −0.15 $km^2\,yr^{-1}$, and lowest for N. Scandinavia −0.01 $km^2\,yr^{-1}$ and W. Canada and W. US −0.01 $km^2\,yr^{-1}$ (see Table 4 for further sub-regional shrinking rates and standard errors).

For the compiled Pan-Arctic GIC in general, the relative shrinkage rate averaged ca. −1 % yr^{-1} (for the last ca. 25 yr) during climate warming, including record high mean annual temperatures for the first decade of the 21st century (2001–2010) (Hansen et al., 2010) (Fig. 10): an average relative shrinkage rate similar to rates reported for high-latitude mountain ranges (Bloch et al., 2010). Overall, this shrinking trend follows the observed mean global GIC mass balance trend towards negative balances

TCD
6, 4417–4446, 2012

(Cogley, 2012), however the mass balance from the most recent pentad (2006–2010) has experienced more moderate, although still large losses.

Randomly chosen observed automatic weather station (AWS) temperature time series were obtained from each of the individual sub-regions, including for GISS/NASA 64° N–90° N latitude band from 1985 through 2011 (Fig. 10). Common for the majority of the displayed AWS was a significant increasing mean annual air temperature (MAAT) (the trend in MAAT is calculated between satellite observations, between the red triangles on Fig. 10), e.g., in parts of Arctic Canada (Ellesmere Island), Greenland, Arctic Russia, and N. and E. Asia: the AWS having a significant increasing MAAT are shown in bold in Table 5. MAAT increased non-uniformly between sub-regions, varying e.g., from $< 0.01\,^{\circ}\mathrm{C\,yr^{-1}}$ in Sandane (S. Scandinavia) to $0.15\,^{\circ}\mathrm{C\,yr^{-1}}$ in Fedorov (Bolshevik Island). For Smithers Airport, W. Canada and W. US, MAAT decreased insignificantly. Besides the regional variability in MAAT, and that MAAT increases significantly at some locations, the Pan-Arctic has in general faced increasing MAAT during the last ca. 25 yr confirmed by the GISS/NASA 64–90° N latitude band time series (see Fig. 10 and Table 5), covering record high MAAT for the first decade of the 21st century (2001–2010) (Hansen et al., 2012).

4 Summary and conclusions

Historically, the representation of shrinking and advancing GIC conditions has been either non-existent or limited for Pan-Arctic regions, however, satellite and aerial observations from SE. Greenland GIC went back to the 1930s (Bjork et al., 2012). Mapping both the present temporal and spatial shrinking and advancing behavior simultaneously of Pan-Arctic GIC provides insight into the climate impacts on the cryosphere. For the last ca. 25 yr shrinking of land-terminating GIC has been documented in high-latitude regions, indicating that GIC have on average lost one-fifth of their area since the mid-1980s (equal to a shrinking rate of ca. $-1\,\%\ \mathrm{yr^{-1}}$), covering a variation in loss rates from 40 % in Alaska to 12 % in Arctic Russia.

TCD
6, 4417–4446, 2012

Acknowledgements. We extent a very special thanks to William H. Lipscomb, Glen E. Liston, Jacob C. Yde, and Matthew W. Hecht for their insightful critique of this article. This work was supported by the Earth System Modeling program within the US Department of Energy's Office of Science and by a Los Alamos National Laboratory (LANL) Director's Fellowship. LANL is operated under the auspices of the National Nuclear Security Administration of the US Department of Energy under Contract No. DE-AC52-06NA25396), and partly from the European Community's Seventh Framework Programme under grant agreement No. 262693. Special thanks are given to the Danish Meteorological Institute (DMI; http://www.dmi.dk) for providing observed air temperature data from the meteorological stations in Thule, Daneborg, Tasiilaq, and Nuuk (Greeenland), Norwegian Meteorological Institute (NMI; http://sharki.oslo.dnmi.no/portal/page?_pageid=73,39035,73_39049&_dad=portal&_schema=PORTAL) for providing data from Bardufoss, Bergen, and Sandane (Norway), Swedish Meteorological and Hydrological Institute (SMHI; http://www.smhi.se) for providing data from Kiruna (Sweden), National Oceanic and Atmospheric Administration (NOAA; http://www.ncdc.noaa.gov/cdo-web/search) for providing data from Talkeetna and Beaver Creek (Alaska), Stampede Pass and Smithers Airport (W. Canada), Eureka (Arctic Canada), Malye Karmakuly, Golomjannyj, and Fedorov (Arctic Russia), and Kijuchi (N. and E. Asia), and National Aeronautics and Space Administration (NASA) for providing temperature data from the Goddard Institute for Space Studies (GISS) database (http://data.giss.nasa.gov/gistemp/tabledata/ZonAnn.Ts+dSST.txt). All satellite data was acquired through the USGS Earth Explorer internet portal (http://earthexplorer.usgs.gov/). Applications for individual GIC area data should be directed to the first author. SHM and JKM compiled the dataset, analyzed the data, and wrote the manuscript. SHM and JKM contributed equally to the study.

References

Arendt, A., Bolch, T., Cogley, J.G., Gardner, A., Hagen, J.-O., Hock, R., Kaser, G., Pfeffer, W. T., Moholdt, G., Paul, F., Radić, V., Andreassen, L., Bajracharya, S., Beedle, M., Berthier, E., Bhambri, R., Bliss, A., Brown, I., Burgess, E., Burgess, D., Cawkwell, F., Chinn, T., Copland, L., Davies, B., de Angelis, H., Dolgova, E., Filbert, K., Forester, R., Fountain, A., Frey, H., Giffen, B., Glasser, N., Gurney, S., Hagg, W., Hall, D., Haritashya, U. K., Hartmann, G., Helm, C., Herreid, S., Howat, I., Kapustin, G., Khromova, T., Kienholz, C., Koenig, M., Kohler, J.,

Kriegel, D., Kutuzov, S., Lavrentiev, I., LeBris, R., Lund, J., Manley, W., Mayer, C., Miles, E., Li, X., Menounos, B., Mercer, A., Moelg, N., Mool, P., Nosenko, G., Negrete, A., Nuth, C., Pettersson, R., Racoviteanu, A., Ranzi, R., Rastner, P., Rau, F., Rich, J., Rott, H., Schneider, C., Seliverstov, Y., Sharp, M., Sigurðsson, O., Stokes, C., Wheate, R., Winsvold, S., Wolken, G., Wyatt, F., and Zheltyhina, N.: Randolph Glacier Inventory [v2.0]: A Dataset of Global Glacier Outlines. Global Land Ice Measurements from Space, Boulder Colorado, USA, Digital Media (http://www.glims.org/RGI/randolph.html), 2012.

Bahr, D. B. and Radić, V.: Significant contribution to total mass from very small glaciers, The Cryosphere, 6, 763–770, doi:10.5194/tc-6-763-2012, 2012.

Bahr, D. B., Dyurgerov, M., and Meier, M. F.: Sea-level rise from glaciers and ice caps: A lower bound, Geophys. Res. Lett., 36, L03501, doi:10.1029/2008GL036309, 2009.

Bjork, A. A., Kjaer, K. H., Korsgaard, N. J., Khan, S. A., Kjeldsen, K. K., Andresen, C. S., Box, J. E., Larsen, N. K., and Funder, S.: An areal view of 80 years of climate-related glacier fluctuations in Southeast Greenland, Natur Geoscience, 5, 427–432, doi:10.1038/NGEO1481, 2012.

Bloch, T., Menounos, B., and Wheate, R.: Landsat-based inventory of glaciers in western Canada, 1985–2005, Remote Sens. Environ., 114, 127–137, 2010.

Brest, C.: Seasonal Albedo of an Urban/Rural Landscape from Satellite Observations, J. Clim. Appl. Meteorol., 26, 1169–1186, 1987.

Cogley, G.: The Future of the World's Glaciers, in: The Future of the World's Climate, edited by: Henderson-Sellers, A. and McGuffie, K., Elsevier, 2012.

Crane, R. G. and Anderson, M. R.: Satellite discrimination of snow/cloud surfaces, Int. J. Remote Sens., 5, 213–223, 1984.

DeBeer, C. M. and Sharp, M. J.: Recent changes in glacier area and volume within the Southern Canadian Cordillera, Ann. Glaciol., 46, 215–221, 2007.

Demuth, M., Pinard, V., Pietroniro, A., Luckman, B., Hopkinson, C., Dornes, P., and Comeau, L.: Recent and Past-century Variations in the Glacier Resources of the Canadian Rocky Mountains: Nelson River System, Terra Glacialis, Special Issue: Mountain Glaciers and Climate Change of the Last Century, 27–52, 2008.

Dozier, J. and Marks, D.: Snow mapping and classification from Landsat Thematic Mapper data, Ann. Glaciol., 9, 97–103, 1987.

Dyurgerov, M. B.: Data of Glaciological Studies – Reanalysis of Glacier Changes: From the IGY to the IPY, 1960–2008, Publication No. 108, Institute of Arctic and Alpine Research (University of Colorado), 2010.
Gao, B.-C.: NDWI – A Normalized Difference Water Index for Remote Sensing of Vegetation Liquid Water From Space, Remote Sens. Environ., 58, 257–266, 1996.
Granshaw, F. D. and Fountain, A. G.: Glacier Change (1958–1998) in the North Cascades national Park Complex, Washington, USA, J. Glaciol., 52, 251–256, 2006.
Grant, K. L., Stokes, C. R., and Evans, I. S.: Identification and characteristics of surge-type glaciers on Novaya Zemlya, Russian Arctic. J. Glaciol., 55, 960–971, 2009.
Hall, D. K., Bayr, K. J., Schoner, W., Bindschadler, R. A., and Chien, J. Y. L.: Consideration of the errors inherent in mapping historical glacier positions in Austria from the ground and space (1893–2001), Remote Sens. Environ., 86, 566–577, 2003.
Hall, D. K., Foster, J. L., Chien, J. Y. L., and Riggs, G. A.: Determination of actual snow covered area using Landsat TM and digital elevation model data in Glacier National Park, Montana, Polar Rec., 31, 191–198, 1995.
Hall, D. K., Riggs, G. A., Salomonson, V. V., DiGirolamo, N. E., and Bayr, K. J.: MODIS snow-cover products, Remote Sens. Environ., 83, 181–194, 2001.
Hansen, J., Ruedy, R., Sato, M., and Lo, K.: Global surface temperature change. Rev. Geophys., 48, RG4004, doi:10.1029/2010RG000345, 2010.
Jiskoot, H., Murray, T., and Luckman, A.: Surge potential and drainage-basin characteristics in East Greenland, Ann. Glaciol., 36, 142–148, 2003.
Kaser, G., Cogley, J. C., Dyurgerov, M. B., Meier, M. F., and Ohmura, A.: Mass balance of glaciers and ice caps: Consensus estimates for 1961–2004, Geophys. Res. Lett., 33, 1–5, 2006.
Kargel, J. S., Ahlstrøm, A. P., Alley, R. B., Bamber, J. L., Benham, T. J., Box, J. E., Chen, C., Christoffersen, P., Citterio, M., Cogley, J. G., Jiskoot, H., Leonard, G. J., Morin, P., Scambos, T., Sheldon, T., and Willis, I.: Brief communication Greenland's shrinking ice cover: "fast times" but not that fast, The Cryosphere, 6, 533–537, doi:10.5194/tc-6-533-2012, 2012.
Liston, G. E.: Interrelationships among Snow Distribution, Snowmelt, and Snow Cover Depletion: Implications for Atmospheric, Hydrologic, and Ecologic Modeling, J. Appl. Meteorol., 38, 1474–1487, 1999.
Luckman, B. H. and Kavavagh, T. Impact of climate fluctuations on mountain environments in the Canadian Rockies, Ambio, 29, 371–380, 2000.

TCD
6, 4417–4446, 2012

Meier, M. F., Dyurgerov, M. B., Rick, U. K., O'neel, S., Pfeffer, W. T, Anderson, R. S., Anderson, S. P., and Glazovsky, A. F.: Glaciers dominate eustatic sea-level rise in the 21st century, Science, 317, 1064–1067, 2007.

Mernild, S. H., Lipscomb, W. H., Bahr, D. B., Radić, V., and Zemp, M.: Imbalance and accelerated melting of glaciers and ice caps, P. Natl. Acad. Sci., in review, 2012a.

Mernild, S. H., Malmros, J. K., Yde, J. C., and Knudsen, N. T.: Multi-decadal marine and land-terminating glacier retreat in Ammassalik region, Southeast Greenland, The Cryosphere, 6, 625–639, doi:10.5194/tc-6-625-2012, 2012b.

Paul, F.: The New Swiss Glacier Inventory 2000 – Application of remote sensing and GIS, Ph.D. thesis, Department of Geography, University of Zurich, 198 pp., 2004.

Post, A.: Distribution of surging glaciers in western North America, J. Glaciol., 8, 229–240, 1969.

Radić, V. and Hock, R.: Regional and global volumes of glaciers derived from statistical upscaling of glacier inventory data, J. Geophys. Res., 115, F01010, doi:10.1029/2009JF001373, 2010.

Radić, V. and Hock, R.: Regionally differentiated contribution of mountain glaciers and ice caps to future sea-level rise, Nature Geosci., 4, 91–94, 2011.

Rouse, J. W., Haas, R. H., Schell, J. A., and Deering, D. W.: Monitoring vegetation systems in the Great Plains with ERTS. Third ERTS Symposium, NASA SP-351, I, 309–317, 1973.

Tennant, C., Menounos, B., and Wheate, R.: Area change of glaciers in the Canadian Rocky Mountains, 1919 to 2006, The Cryosphere Discuss., 6, 2327–2361, doi:10.5194/tcd-6-2327-2012, 2012.

Weidick, A., Bøggild, C. E., and Knudsen, N. T.: Glacier inventory of west Greenland, Boulder, CO: National Snow and Ice Data Center, Digital media, 1992.

World Glacier Monitoring Service, Glacier Mass Balance Bulletin No. 11 (2008–2009), edited by: Zemp, M., Nussbaumer, S. U., Gärtner-Roer, I., Hoelzle, M., Paul, F., and Haeberli, W., (ICSU(WDS)/IUGG(IACS)/UNEP/UNESCO/WMO, 2011.

Yde, J. C. and Knudsen, N. T.: 20th-century glacier fluctuation on Disko Island (Qeqertarsuaq), Greenland. Ann. Glaciol., 46, 209–214, 2007.

TCD
6, 4417–4446, 2012

Table 1. Satellite platform, sensors, band information, scenes used in the analysis, and precision errors. A geographical distribution of the sub-regions can be seen in Fig. 1.

Sub-region	Platform	Sensor and bands	Ground resolution (meters)	Precision error (meters)	Scenes	Survey years and dates (yyyyddmm)
Alaska	Landsat-5	TM (bands 1–5, and 7)	30 × 30	± 15	LT50700161987233XXX02	19872108
	Landsat-5	TM (bands 1–5, and 7)	30 × 30	± 15	LT50700162007240GLC00	20072808
W. Canada and W. US	Landsat-5	TM (bands 1–5, and 7)	30 × 30	± 15	LT50510231985270PAC00	19852709
	Landsat-5	TM (bands 1–5, and 7)	30 × 30	± 15	LE70510232011254EDC00	20111109
Ellesmere Island	Landsat-5	TM (bands 1–5, and 7)	30 × 30	± 15	LT50450051988205PAC00	19882307
	Landsat-5	TM (bands 1–5, and 7)	30 × 30	± 15	LT50450052009214GLC00	20090208
NE. Greenland	Landsat-5	TM (bands 1–5, and 7)	30 × 30	± 15	LT52310061985219XXX03	19850708
	Landsat-5	TM (bands 1–5, and 7)	30 × 30	± 15	LT52310062009221KIS00	20090908
SE. Greenland	Landsat-5	TM (bands 1–5, and 7)	30 × 30	± 15	LT52310141986254XXX03	19860911
	Landsat-7	ETM+ (bands 1–5, and 7)	30 × 30	± 15	LE72320132011226EDC01	20111408
					LE72320142011226EDC00	20111408
					LE72310142007256EDC00	20070409
SW. Greenland	Landsat-5	TM (bands 1–5, and 7)	30 × 30	± 15	LT50050151987242XXX03	19873008
	Landsat-7	ETM+ (bands 1–5, and 7)	30 × 30	± 15	LE70070152003260EDC02	20041709
	Landsat-7	ETM+ (bands 1–5, and 7)	30 × 30	± 15	LE70070152004247EDC02	20030409
NW. Greenland	Landsat-5	TM (bands 1–5, and 7)	30 × 30	± 15	LT50370021987226XXX01	19871408
	Landsat-5	TM (bands 1–5, and 7)	30 × 30	± 15	LT50380022006221KIS00	20060908
N. Scandinavia	Landsat-5	TM (bands 1–5, and 7)	30 × 30	± 15	LT51970121987227XXX01	19871508
	Landsat-5	TM (bands 1–5, and 7)	30 × 30	± 15	LE71960122006232ASN00	20061908
S. Scandinavia	Landsat-5	TM (bands 1–5, and 7)	30 × 30	± 15	LT52000171988219KIS00	19880608
	Landsat-5	TM (bands 1–5, and 7)	30 × 30	± 15	LT51990172011259MOR00	20110609
Novaya Zemlya	Landsat-5	TM (bands 1–5, and 7)	30 × 30	± 15	LT51770081987215XXX02	19870308
	Landsat-7	ETM+ (bands 1–5, and 7)	30 × 30	± 15	LE71780082011232ASN00	20112008
	Landsat-7	ETM+ (bands 1–5, and 7)	30 × 30	± 15	LE71780082011248ASN00	20110509
Bolshevik Island	Landsat-5	TM (bands 1–5, and 7)	30 × 30	± 15	LT51570041985213XXX02	19850108
	Landsat-7	ETM+ (bands 1–5, and 7)	30 × 30	± 15	LE71600032011234PFS00	20112208
Kamchatka	Landsat-5	TM (bands 1–5, and 7)	30 × 30	± 15	LE70990201999222EDC00	19991008
	Landsat-5	TM (bands 1–5, and 7)	30 × 30	± 15	LT50990202011215MGR00	20110308

TCD
6, 4417–4446, 2012

Table 2. Sub-regional raw classification error due to a comparison with the cleaned up classification. The snow patch error was overestimated for all sub-regions, and the debris and shadow error underestimated for all sub-regions.

Sub-region	Snow patch error (%)	Debris cover and shadow error (%)	Overall classification shadow error (%)
Alaska	3.0	3.2	6.2
W. Canada and W. US	2.9	3.1	6.0
Ellesmere Island	2.5	1.2	3.7
NE. Greenland	2.7	1.9	4.6
SE. Greenland	3.4	1.8	5.2
SW. Greenland	3.3	2.5	5.8
NW. Greenland	2.7	1.9	2.7
N. Scandinavia	3.1	1.5	4.6
S. Scandinavia	3.7	1.6	5.3
Novaya Zemlya	5.3	3.3	5.3
Bolshevik Island	2.2	0.7	2.9
Kamchatka	3.9	2.1	6.0
Average	3.0	1.9	4.9

TCD
6, 4417–4446, 2012

Table 3. The compiled Landsat GIC data set were divided into seven first-order Pan-Arctic regions. For N. and E. Asia the satellite period was shorter than other regions, covering the period 1999–2011.

First-order regions	Numbers of GIC (n)	Period (years)	The percentage of advancing GIC (%)	Mean GIC area change and standard error (%)	Mean GIC area change and standard error ($km^2\,yr^{-1}$)
Alaska	26	1987–2011 (24)	0	-40 ± 4 (-1.7 % yr^{-1})	-0.04 ± 0.01
W. Canada and W. US	31	1985–2011 (26)	13	-12 ± 3 (-0.5 % yr^{-1})	-0.01 ± 0.00
Arctic Canada (Ellesmere Island)	32	1988–2009 (21)	0	-35 ± 4 (-1.7 % yr^{-1})	-0.15 ± 0.03
Greenland*	104	1985–2011 (26)	8	-20 ± 2 (-0.8 % yr^{-1})	-0.07 ± 0.01
Scandinavia (North and South)	60	1987–2011 (24)	0	-21 ± 2 (-0.9 % yr^{-1})	-0.02 ± 0.01
Russian Arctic (Novaya Zemlya and Bolshevik Island)	47	1985–2011 (26)	26	-12 ± 2 (-0.5 % yr^{-1})	-0.10 ± 0.02
N. and E. Asia (Kamchatka)	21	1999–2011 (12)	10	-23 ± 3 (-1.9 % yr^{-1})	-0.04 ± 0.01
Pan-Arctic	321		8	-21 ± 1 (~ -1 % yr^{-1})	-0.06 ± 0.01

* SE. Greenland GIC data have been published in Mernild et al. (2012b).

TCD
6, 4417–4446, 2012

Table 4. The compiled Landsat GIC data set were divided into twelve Pan-Arctic regions.

Sub-regions	Numbers of GIC (n)	Period (years)	The percentage of advancing GIC (%)	Mean GIC area change and standard error (%)	Mean GIC area change and standard error ($km^2 yr^{-1}$)
Alaska	26	1987–2011 (24)	0	-40 ± 4 ($-1.7\,\%\,yr^{-1}$)	-0.04 ± 0.01
W. Canada and W. US	31	1985–2011 (26)	13	-11 ± 3 ($-0.4\,\%\,yr^{-1}$)	-0.01 ± 0.00
Ellesmere Island	32	1988–2009 (21)	0	-35 ± 4 ($-1.7\,\%\,yr^{-1}$)	-0.15 ± 0.03
NE. Greenland	29	1985–2009 (24)	0	-20 ± 3 ($-0.8\,\%\,yr^{-1}$)	-0.05 ± 0.03
SE. Greenland*	35	1986–2011 (25)	9	-27 ± 4 ($-1.1\,\%\,yr^{-1}$)	-0.03 ± 0.01
SW. Greenland	17	1987–2003 (16)	37	-8 ± 3 ($-0.5\,\%\,yr^{-1}$)	-0.02 ± 0.01
NW. Greenland	23	1987–2006 (19)	0	-19 ± 3 ($-1.0\,\%\,yr^{-1}$)	-0.18 ± 0.05
N. Scandinavia	29	1987–2006 (19)	0	-19 ± 2 ($-1.0\,\%\,yr^{-1}$)	-0.01 ± 0.00
S. Scandinavia	31	1988–2011 (23)	0	-22 ± 2 ($-1.0\,\%\,yr^{-1}$)	-0.03 ± 0.01
Novaya Zemlya	21	1987–2011 (24)	5	-15 ± 2 ($-0.6\,\%\,yr^{-1}$)	-0.16 ± 0.03
Bolshevik Island	26	1985–2011 (26)	42	-9 ± 4 ($-0.3\,\%\,yr^{-1}$)	-0.05 ± 0.02
Kamchatka	21	1999–2011 (12)	10	-23 ± 3 ($-1.9\,\%\,yr^{-1}$)	-0.04 ± 0.01
Pan-Arctic	321		8	-21 ± 1 ($\sim -1\,\%\,yr^{-1}$)	-0.06 ± 0.01

* SE. Greenland GIC data have been published in Mernild et al (2012b).

TCD
6, 4417–4446, 2012

Table 5. GISS/NASA and AWS observed MAAT trends for the individual sub-regions are shown for the satellite observation periods (the locations of the AWS are illustrated on Fig. 10). Significant trends are highlighted in bold. The abbreviations indicate: NOAA (National Oceanic and Atmospheric Administration), DMI (Danish Meteorological Institute), SMHI (Swedish Meteorological and Hydrological Institute), NMI (Norwegian Meteorological Institute), and NASA (National Aeronautics and Space Administration).

Sub-region	AWS	Satellite observation period	MAAT trend ($^{\circ}$C yr^{-1})	Source
Alaska	Talkeetna	1987–2011	0.04	NOAA
Alaska	Beaver Creek	1987–2011	0.01	NOAA
W. Canada and W. US	Stampede Pass	1985–2011	**0.05**	NOAA
W. Canada and W. US	Smithers Airport	1985–2011	−0.01	NOAA
Ellesmere Island	Eureka	1988–2009	**0.09**	NOAA
NE. Greenland	Danmarkshavn	1985–2009	**0.08**	DMI
SE. Greenland	Tasiilaq	1986–2011	**0.08**	DMI
SW. Greenland	Nuuk	1987–2003	**0.10**	DMI
NW. Greenland	Thule	1987–2006	**0.12**	DMI
N. Scandinavia	Kiruna	1987–2006	**0.07**	SMHI
N. Scandinavia	Bardufoss	1987–2006	0.03	NMI
S. Scandinavia	Bergen	1988–2011	0.02	NMI
S. Scandinavia	Sandane	1988–2011	<0.01	NMI
Novaya Zemlya	Malye Karmakuly	1987–2011	**0.08**	NOAA
Bolshevik Island	Golomjannyj	1985–2011	**0.14**	NOAA
Bolshevik Island	Fedorov	1985–2011	**0.15**	NOAA
Kamchatka	Kljuchi	1999–2011	**0.11**	NOAA
64° N to 90° N	GISS/NASA	1985–2011	**0.08**	NASA

TCD
6, 4417–4446, 2012

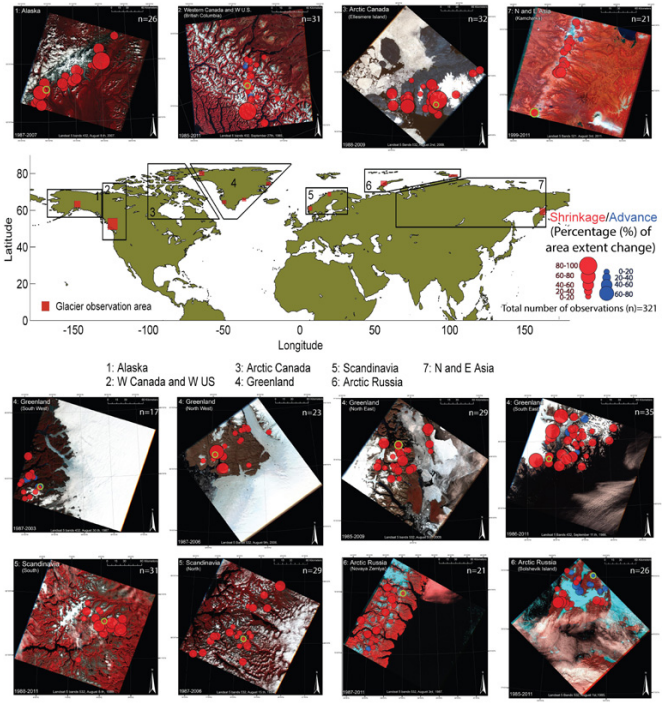

Fig. 1. Satellite-derived area changes of 321 GIC in the Pan-Arctic. Changes are shown as rates during the observation period from ca. mid-1980s to late 2000s/2011 (the period varies between regions, and for N. and E. Asia the observation period was 1999 to 2011). The data were divided into seven first-order glaciated regions: **(1)** Alaska, **(2)** W. Canada and W. US, **(3)** Arctic Canada, **(4)** Greenland, **(5)** Scandinavia, **(6)** Arctic Russia, and **(7)** N. and E. Asia. Three of the first-order regions were divided into sub-regions illustrated on the Landsat images, indicating in total 12 sub-regions. Red circles show GIC shrinkage and blue circles advance (percentage, %). Circles with green margin show examples of GIC margin and area changes illustrated in Fig. 8. Background satellite images are from Landsat-5 TM.

TCD
6, 4417–4446, 2012

S. H. Mernild and J. K. Malmros

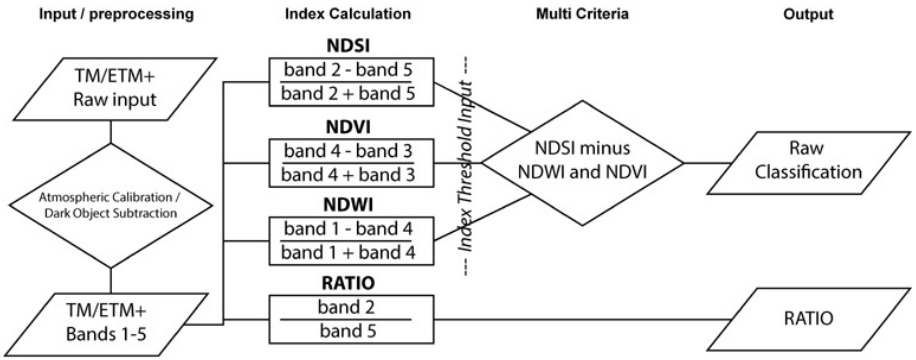

Fig. 2. A schematic diagram of the workflow for the classification of Landsat images, where the trapeze shapes indicates steps where input data were added or output data generated, and the diagram shapes indicates steps where processing of data were done.

TCD
6, 4417–4446, 2012

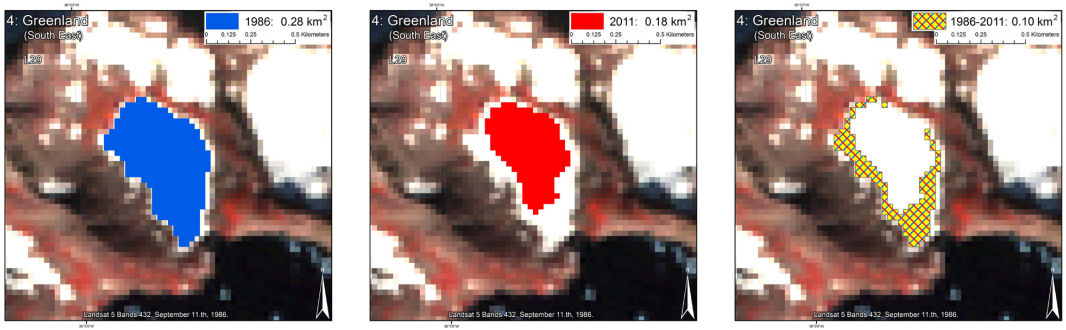

Fig. 3. An example of the margin positions for the glacier L29, SE. Greenland, for 1986 (blue) and 2011 (red), and the 1986 to 2011 area change (yellow shaded) (the location of glacier L29 can be seen in Mernild et al., 2012b, Fig. 1).

TCD
6, 4417–4446, 2012

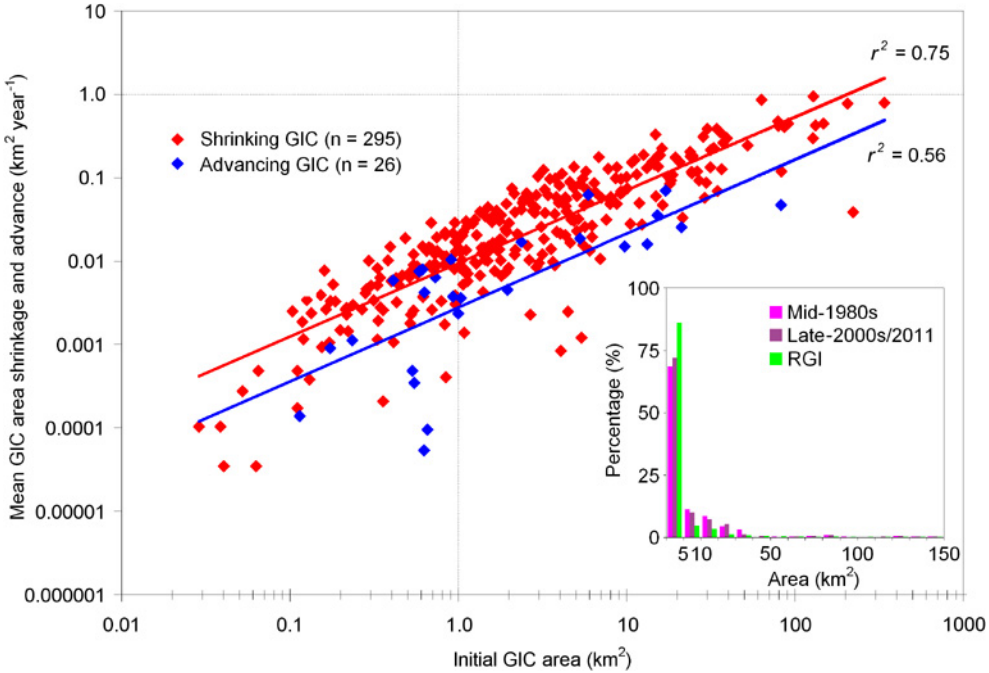

Fig. 4. Relationship for advancing GIC (blue diamonds) and shrinking GIC (red diamonds), and their initial area versus area change. The initial GIC area is based on data from mid-1980s, and the area rate is the annual area difference between mid-1980s and late-2000s/2011. The inset histogram illustrates the GIC area distribution for the mid-1980s compiled data set, the late-2000s/2011 compiled data sets, and for the Randolph Glacier Inventory (RGI) data set between 52.4° N and 89.3° N latitude (Arendt et al., 2012).

TCD
6, 4417–4446, 2012

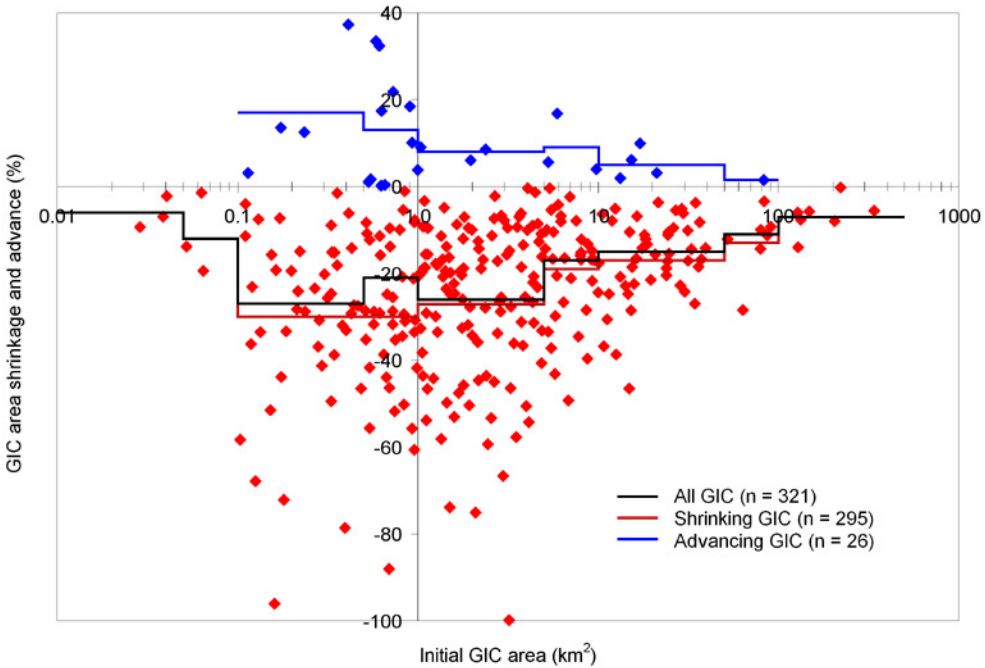

Fig. 5. Relationship for advancing GIC (blue diamonds) and shrinking GIC (red diamonds), and their initial area versus the percentage of area change. The initial GIC area is based on data from mid-1980s, and the area rate is the percentage annual area difference between mid-1980s and late-2000s/2011. The bold lines (black, red, and blue) illustrate the mean percentage of area change for the intervals: 0.01–0.05, 0.05–0.1, 0.1–0.5 etc.

TCD
6, 4417–4446, 2012

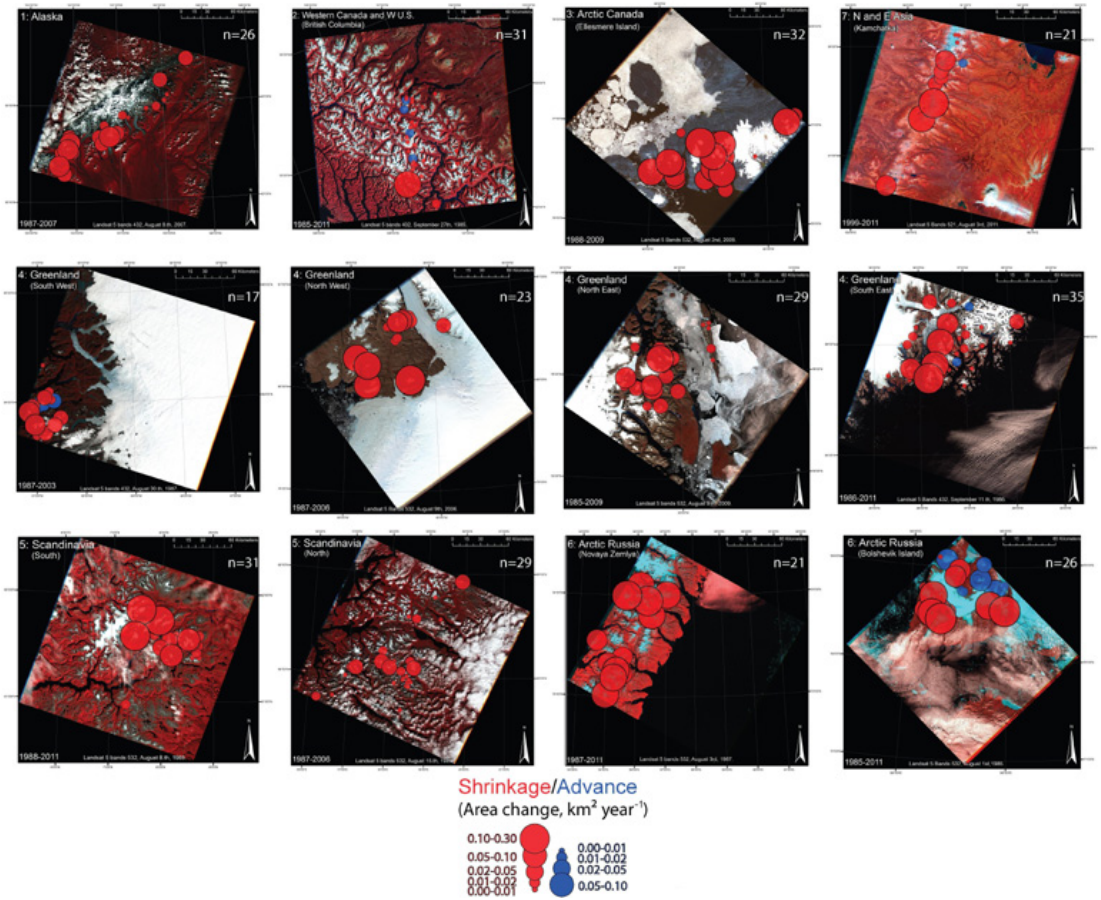

Fig. 6. Satellite-derived area change rates for GIC within the 12 sub-regions, where red circles show GIC shrinkage and blue circles advance ($km^2\ yr^{-1}$). Background satellite images are from Landsat-5 TM.

TCD
6, 4417–4446, 2012

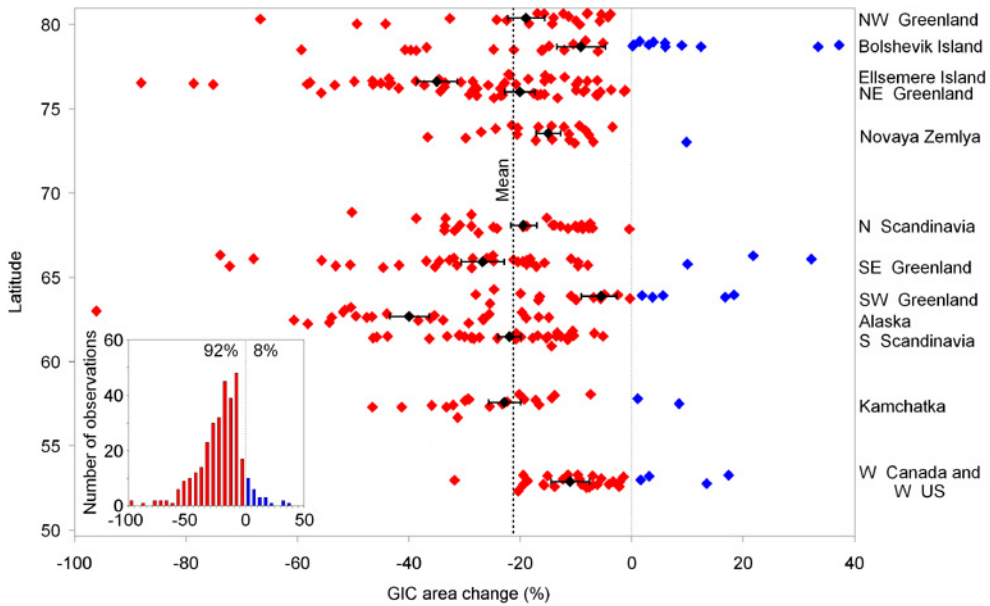

Fig. 7. Area changes for the twelve sub-regions where each diamond represents each individual GIC. GIC are plotted against latitude. Red diamonds show GIC shrinkage and blue diamonds advance. Black diamonds illustrates the sub-region mean area change and the bars reflect one standard error. The dotted line illustrated the arithmetic mean. The histogram depicts the different distribution in GIC area change rates.

TCD
6, 4417–4446, 2012

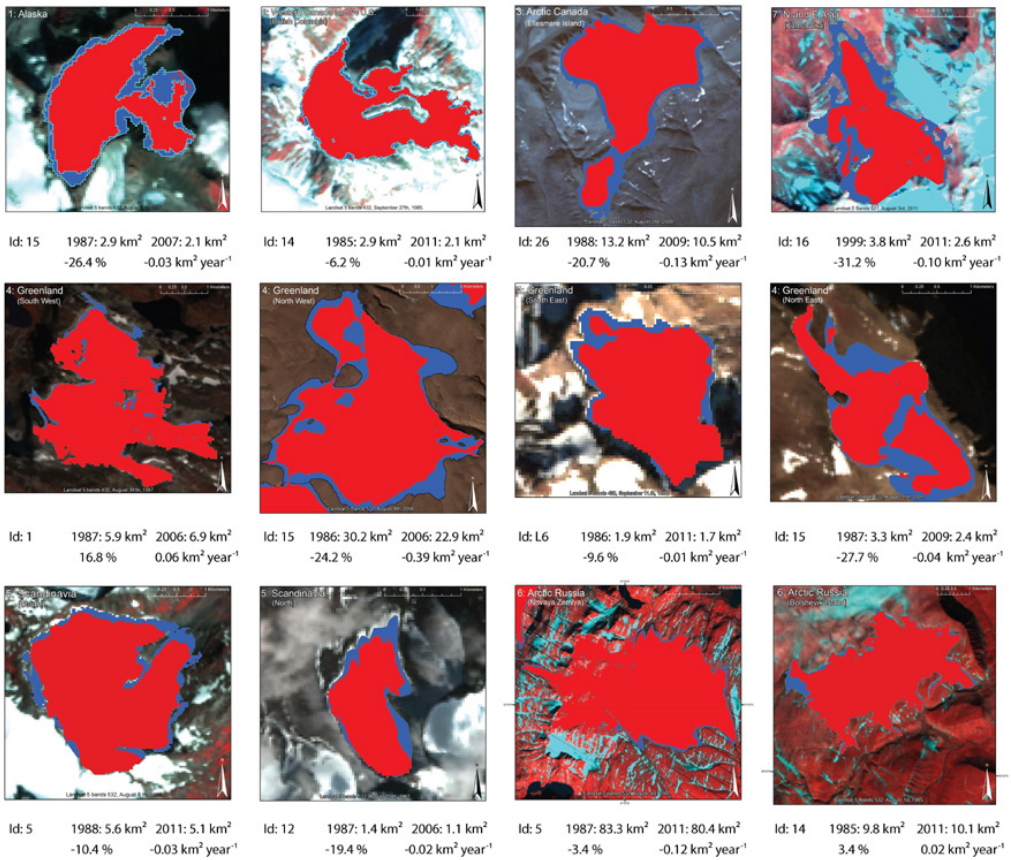

Fig. 8. Examples of satellite-derived margin location and area changes of twelve chosen GIC (for both minor and major GIC; one GIC for each sub-region) for the period mid-1980s (blue) to late-2000s/2011 (red) estimated from Landsat images. The location of the GIC is shown in Fig. 1.

TCD
6, 4417–4446, 2012

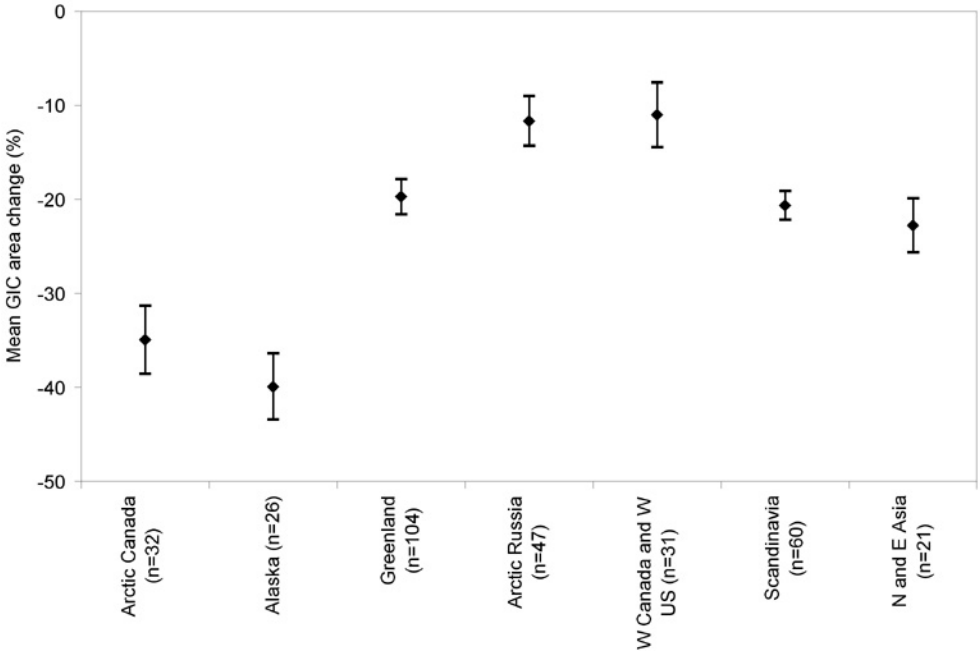

Fig. 9. Arithmetic mean values of area changes for each of seven first-order glaciated regions from mid-1980s to late-2000s/2011 (for N. and E. Asia the observation period spans the period from 1999 to 2011). The number of GIC per first-order region is shown in parentheses. The bars denote one standard error in each direction; regions with few GIC have the largest standard error.

TCD
6, 4417–4446, 2012

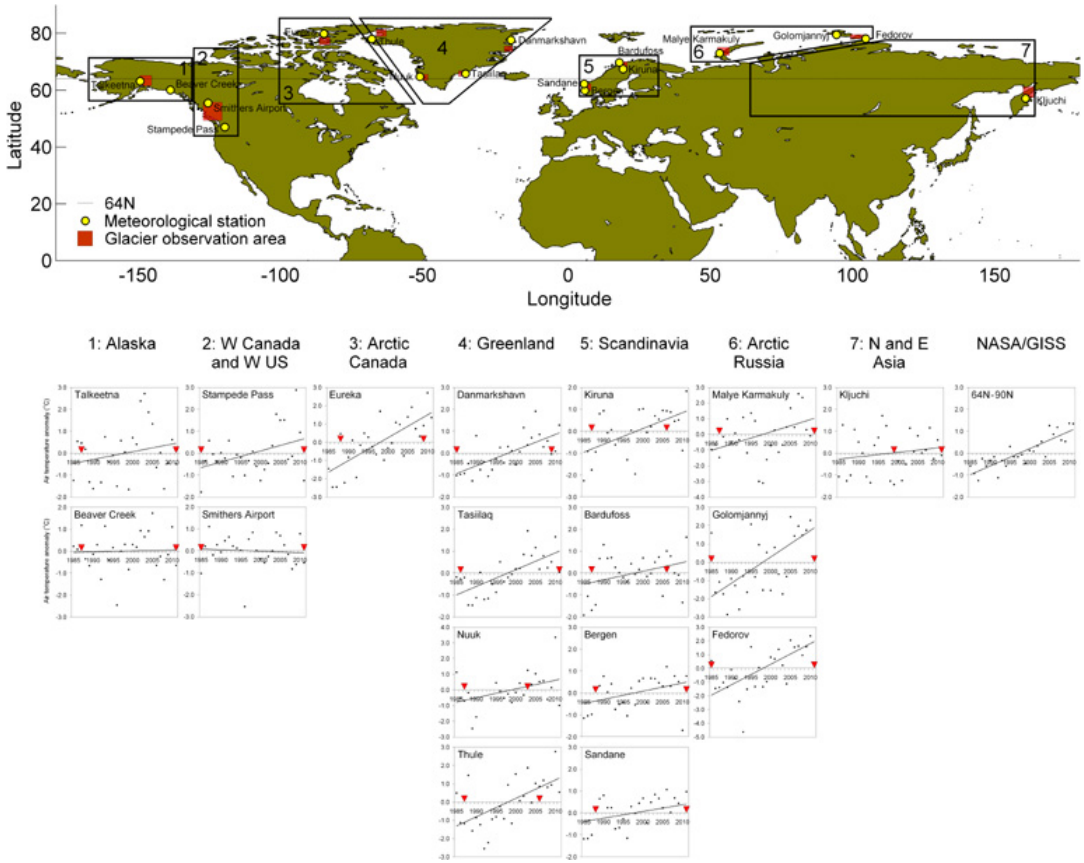

Fig. 10. Examples of AWS observed MAAT omaly time series from different locations in the individual sub-regions (1985–2011), including MAAT anomaly time series tracked through the National Aeronautics and Space Administration (NASA) Goddard Institute for Space Studies (GISS) for the latitude band 90–64° N. The period with GIC satellite observations is marked for each air temperature time series (see red triangles).

TCD
6, 4417–4446, 2012